Late Diagenesis of Illite-Smectite in the Podhale Basin: Chemistry, Morphology and Preferred Orientation

Ruarri J. Day-Stirrat[1*], Andrew C. Aplin[2], Kuncho D. Kurtev[3], Anja M. Schleicher[4], Andrew P. Brown [5] and Jan Środoń[6]

[1] Shell International E&P Inc, Shell Technology Center-Houston, 3333 Highway 6 South, Houston, Tx, 77082, USA

[2] Department of Earth Sciences, Durham University, Durham, DH1 3LE, U.K. a.c.aplin@durham.ac.uk

[3] SINTEF, Sem Sælands vei 11, 7034, Trondheim, Norway. Kuncho.Kurtev@sintef.no

[4] Helmholtz Centre Potsdam,GFZ German Research Centre for Geosciences, Telegrafenberg, Building B, room 327, 14473 Potsdam, Germany. anja.maria.schleicher@gfz-potsdam.de

[5] Institute for Materials Research, University of Leeds, Leeds, LS2 9JT, UK. A.P.Brown@leeds.ac.uk

[6] Institute of Geological Sciences, PAN, Senacka 1, 31-002 Kraków, Poland ndsrodon@cyf-kr.edu.pl

*Corresponding Author:

Dr. Ruarri J. Day-Stirrat

Shell International E&P Inc, Shell Technology Center-Houston, 3333 Highway 6 South, Houston, Tx, 77082, USA

E-mail: ruarri.day-stirrat@shell.com

Abstract

Well-characterized samples from the Podhale Basin, southern Poland, formed the basis for exploring and illuminating subtle diagenetic changes to a mudstone towards the upper end of the diagenetic window, prior to metamorphism. Transmission Electron Microscopy (TEM) performed on dispersed grains and ion-beam thinned preparations, Selected Area Diffraction Patterns (SAED) and chemistry by TEM-EDS (Energy Dispersive Spectra) augmented mineralogy and fabric data. The deepest samples show no change in their percent illite in illite-smectite (I-S), yet I-S phase octahedral Fe^{3+} and Al^{3+} are statistically different between samples. A decrease in the in the Fe^{3+} concentration in the octahedral sheet correlates with an increase in I-S fabric intensity and apparent crystallinity. The D-statistic from the Kolmogorov-Smirnov (K-S) test on TEM-EDS data describes statistical differences between the I-S chemistry. Previous work on these samples showed a significant increase in the preferred orientation of the I-S phase across the smectite-to-illite transition and a significant slowdown in the rate of development of preferred orientation beyond the termination of smectite illitization. Lattice fringe images describe an I-S morphology that coalesces into large and tighter packets with increasing burial temperature and a decrease in I-S packet contact angle, yet some evidence for smectite collapse structures is retained. The deepest sample shows the thickest, most coherent I-S packets. We propose that the deepest samples in the Podhale Basin describe the precursor stage in phyllosilicate fabric preferred orientation increase from diagenesis into metamorphism, where continued evolution of crystallite packets and associated crystallinity create higher I-S fabric intensities as the structural formulae of I-S approaches an end-member composition.

Keywords: Late-diagenesis; Illite-smectite; Micro-Fabric; Shale; Mudstone

1. Introduction

The physical, chemical and mineralogical changes which transform muds into mudstones and ultimately metamorphic pelites have been studied for many years (Sorby, 1853; Rieke and Chilingarian, 1974; Weaver, 1989; Bjørlykke and Høeg, 1997). With respect to mineralogical change, particular attention has been paid to the major reactions involving clay minerals, most obviously the transformation of smectite to illite and additional mineral changes, for example quartz and chlorite precipitation, associated with that reaction (e.g. Perry and Hower, 1970; Hower et al., 1976; Boles and Franks, 1979; Nadeau et al., 2002). Whilst X-ray diffraction has charted the mineralogical changes, Transmission Electron Microscopy (TEM) has been used to examine the microstructural and chemical changes involved not only in the smectite to illite transformation (Ahn and Peacor, 1986; Bell, 1986; Klimentidis and Mackinnon, 1986; Inoue et al., 1987a; Inoue et al., 1987b; Jiang et al., 1994; Hover et al., 1999; Masuda et al., 2001; Nadeau et al., 2002; Kim et al., 2004), but also in the reactions involved in low grade metamorphism (Merriman and Peacor, 1998; Merriman, 2002).

Other work has focused on the processes by which the initially random arrangement of phyllosilicate minerals in mud becomes organized into the highly aligned fabric observed in metapelites (Oertel and Curtis, 1972; Curtis et al., 1980; Ho et al., 1999; Jacob et al., 2000; Aplin et al., 2006; Day-Stirrat et al., 2008a; Day-Stirrat et al., 2008b). Discussion has centered on the relative roles of mechanically-driven rearrangement of particles and mineralogical changes in which neoformed phyllosilicate minerals grow normal to the principal effective stress. Whilst laboratory compaction experiments show that mechanical rearrangement of phyllosilicates is feasible (Djéran-Maigre et al., 1998; Haines et al., 2009; Voltolini et al., 2009; Day-Stirrat et al., 2011), both Ho et al. (1999) and Day-Stirrat et al. (2008a) observed a major enhancement to the

preferred orientation of I-S across the smectite to illite transition in the Gulf of Mexico and the Podhale Basin of southern Poland, respectively. Day-Stirrat et al. (2008a) suggested that the enhanced fabric intensity through the smectite to illite transition window was indicative of dissolution of smectite and growth of new illite perpendicular to principal effective stress.

The changes in phyllosilicate fabric observed at the end of the main smectite to illite transition are nevertheless substantially lower than those observed in low grade metapelites (Jacob et al., 2000). This implies continuing rearrangement of fabric at temperatures and stresses higher than those associated with the smectite illitization. In contact metamorphism, enhancement of phyllosilicates fabrics close to the heating body have been recorded (Ho et al., 1995). In the Podhale Basin (Figure 1), Day-Stirrat et al.'s (2008a) data tentatively suggested a continued increase in I-S (and chlorite) fabric intensity beyond the apparent termination of the smectite to illite transition or certainly the mineral reaction slowdown (Figure 2). This slowdown occurs over an additional burial of 2 km and a temperature increase of 40°C (approximately 115°C to 150°C). Since the porosity of these deeply buried samples is low and pore sizes are smaller than grains, increases in the alignment of phyllosilicate grains are unlikely to result from mechanical processes, but rather from dissolution and reprecipitation processes which may be revealed by changes in I-S chemistry or microfabric. Changes in mineral chemistry have implications for density, and microfabric impacts anisotropy and velocity. The practical importance of these changes is that both density and velocity are key parameters in estimating both porosity and pore pressure in mud-rich sequences, particularly in circumstances where sediments have been unloaded (Bowers, 1995; Lahann and Swarbrick, 2011; Goulty and Sargent, 2016; Goulty et al., 2016). Since relationships between vertical effective stress (VES) and porosity/density are difficult to constrain in diagenetically mature samples (Yang and Aplin, 2004), an examination of the detailed chemistry of mineral change in a low porosity system is timely.

In this study, therefore, we take some well-characterized samples from the deepest part of the Podhale Basin and perform transmission electron microscopy (TEM) on both dispersed grains and ion-beam thinned preparations. The TEM-EDS data allow us to look for compositional changes at and beyond the smectite to illite transition, whilst lattice fringe images allow a visual description of the change in crystallite morphology, thickness and fabric. The samples in this paper thus represent a part of the journey a mud takes on its journey to a metamorphic pelite.

2. Geological setting and data background

The Palaeogene Podhale Basin of southern Poland is situated between the Pieniny Klippe Belt to the north and the Tatra Mountains to the south (Figure 1). The basin is filled with what is termed the Podhale Flysch (Olszewska and Wieczorek, 1998), deposited by submarine fans (Westwalewicz-Magilska, 1986) and covering a Mesozoic basement that is exhumed in the Tatra Mountains.

X-ray diffraction results (Table 1) on the Palaeogene mudstones (Środoń et al., 2006a) describe an extremely homogeneous detrital mineral composition, with regular and clear diagenetic trends with depth. Based on grain-density trends Środoń et al. (2006b) argue that two wells, Chochołów PIG-1 and Bukowina Tatrzańska PIG-1, can be seen as a continuous burial profile, in which a ~500m overlap produces a continuous trend in percentage of smectite in the mixed-layer phase illite-smectite, as well as predictable increases in quartz and chlorite and decreases in kaolinite and potassium feldspar. Present day and calculated palaeo-geothermal gradients are similar in both wells (~20-25ºC km^{-1}). The overlap proposed by Środoń et al (2006b) is consistent with thermal maturity data from Poprawa and Marynowski (2005). The maximum burial of the Podhale Basin was achieved at ~17 Ma, based on K-Ar dates from clay mineral separates from bentonites (Środoń et al., 2006b) and maximum burial was deeper than present day

burial. Marynowski et al. (2006) present a burial history profile through the center of the basin that shows rapid Oligocene burial followed by Miocene uplift. Porosity data recorded by Day-Stirrat et al. (2008a) show a consistent decrease through the established synthetic profile. The area was the subject of an apatite fission track analysis by Anczkiewicz (2006), who also concluded that the top of Bukowina Tatrzańska PIG-1 had previously been much deeper (totally reset tracks) than the top of Chochołów PIG-1 (partially reset tracks) and subsequently it was eroded.

The smoothness of the diagenetic trends (Środoń et al., 2006b), the continuity of physical trends in grain density (Środoń et al., 2006b), phyllosilicate preferred orientation and porosity (Day-Stirrat et al., 2008a) and rapid burial and uplift (Anczkiewicz, 2006) suggest that the submarine fan depositional system described by Westwalewicz-Magilska (1986) was fed by a consistent source area over the period of deposition. The rapid burial of the fore-arc basin system (Tari et al., 1993) of the Podhale flysch probably mitigated significant progradation of the submarine fans leading to the consistent trends noted above, due to a consistent provenance.

3. Samples and Methods

3.1 Samples

The sample set consists of four fragments of cores selected from two boreholes in the Podhale Basin (Figure 1): Chochołów PIG-1 in the west (samples Chochołów-06 and Chochołów-60) and Bukowina Tatrzańska PIG-1 in the east (Bukowina Tatrzańska-06 and Bukowina Tatrzańska-41). These samples cover a maximum temperature and depth range of ~ 50 - 150 °C and 2500 – 7000 m original depth of burial (Table 1). Additional detailed sample information can be found in Marynowski et al. (2006), Środoń et al. (2006b) and Day-Stirrat et al. (2008a). Sample

Chochołów-06 has 50% illite in illite-smectite whereas, Chochołów-60, Bukowina Tatrzańska-06, and Bukowina Tatrzańska-41 all have 76% illite in illite-smectite.

3.2 Transmission Electron Microscopy

Chemistry of individual illite-smectite phyllosilicate particles was determined using TEM-EDS; crystallite images and selected area diffraction patterns (SAED) were also obtained. Samples were examined at the University of Leeds using a Philips/FEI CM200 electron microscope equipped with a Field Emission Gun (FEG), and a Gatan Imaging Filter (GIF). The extinction voltage was set at 3.21 kV, giving a typical energy resolution of 0.8 eV.

Mudstone samples were disaggregated using a gentle freeze-thaw method which does not crush individual particles (Yang and Aplin, 1997). The less than 2μm fraction of the sample was then separated by centrifugation. Selected < 2μm fractions were prepared for TEM-EDS by dispersing 0.2 g of sample in excess ethanol. Approximately 10μL of the dilute suspension was placed on a carbon coated 200-mesh copper grid and allowed to evaporate to dryness. This technique assumes that phyllosilicate particles are aligned with (00*l*) planes approximately perpendicular to the electron beam (c* parallel to beam). Care was taken to obtain SAED patterns from thin grains, free from the overlap of other grains. Magnification was at 50,000x and Energy Dispersive Spectra (EDS) data were acquired at between 1000 and 3000 counts per second with a live time of 50 seconds using a 75Å beam diameter on the same spot as the SAED. Biotite and paragonite standards were used to obtain K-factors for the transformation of intensity ratios to concentrations (Cliff and Lorimer, 1975). Oxygen was not measured as it is strongly affected by differences in sample thickness. Atomic concentration ratios were converted into normalized mineral formulae using an anionic charge of 22 ($O_{10}[OH]_2$) and assuming that all iron occurs as Fe^{3+} (Weaver, 1989; Moore and Reynolds, 1997). Oxide weight percents were calculated by

normalizing the atomic ratios to 95 wt% (Merriman et al., 1995). Since alkali loss, particularly potassium, is a significant problem in TEM-EDS analysis (van der Pluijm et al., 1988), a consistent 50 second count time was used for all samples. A loss of potassium was assumed and the sodium content was not included in the normalization calculations. Omitting Na^{+} from the mineral formula does not seriously affect interlayer charge as it comprises <0.1 cations per unit formula. All Mg^{2+} and Fe^{3+} were assigned to the octahedral sheet. Estimated uncertainties in the atomic proportions are: Si^{4+} and Al^{3+}, ~ ± 0.1 cations per unit formula; Fe^{3+}, Mg^{2+}, Ti^{4+}, ~ ± 0.05 cations per unit formula; K^{+}, ~ ± 0.2 cations per unit formula (Peacor, 1992; Warren and Ransom, 1992).

A thin-section previously prepared for backscattered electron imaging (Day-Stirrat et al. 2008a) produced a sample stub that was cut 200-400μm for high resolution X-ray texture goniometry (Day-Stirrat et al., 2008a). The same sample stub was prepared for lattice fringe imaging with a L.R. White resin treatment (Kim et al., 1995) and was used prior to sample preparation in order to prevent the collapse of smectite layers in the high vacuum environment of the TEM. The preparation aimed to look at I-S in its a or b planes (c* perpendicular to beam). TEM in this mode has the ability to image the size of crystallite packets and document layer terminations between crystallites. Three millimeter diameter aluminum washers were attached to randomly selected areas on the prepared TEM thin-section and the sample was ion-beam thinned and carbon coated for TEM observation. Lattice fringe observations were obtained using a Phillips CM12 Scanning Transmission Electron Microscope (STEM) at the University of Michigan. The STEM was operated at an accelerating voltage of 120 kV and a beam current of ~10 nA.

3.3 Statistical Analysis (Kolmogorov-Smirnov test)

The Kolmogorov-Smirnov test (K-S Test) is a method that expresses the similarity or difference between two datasets (Stuart et al., 1999). The test was used on TEM-EDS data from

191 the Podhale Basin samples. The K-S Test is non-parametric and does not require a particular
192 distribution of data (e.g. data normally distributed). It can be used on small datasets (8-13 results),
193 where simply presenting the arithmetic average of a result implies a normal distribution, and also
194 enables the K-S test a visual appraisal of the similarity of datasets. For a dataset of 20 points, the
195 test is very simple but powerful, the data are ordered and the lowest value plotted at 0.05 (1/20);
196 the second lowest value would be plotted at 0.1 (2/20), and so on up to 1 to complete the cumulative
197 distribution. Distributions can be compared visually, and a D-statistic is calculated as the
198 maximum difference or separation between two cumulative distributions and expressed as a
199 percentage.
200
201 **4. Results**
202 **4.1 Selected Area Diffraction Patterns (SAED)**
203 Morphologies of grains for which selected area diffraction patterns were obtained range
204 from euhedral crystallites (Figure 3) to subhedral crystallites (Figure 4). The associated SAED
205 patterns, taken at thin edges of crystallites, have a strong hexagonal arrangement of single crystal
206 diffraction spots in all samples. These spots correspond to (*h*,*k*,*l*) reflections. The presence of sharp
207 hexant reflections implies coherence between individual layers, and the absence of diffuse
208 diffraction rings is consistent with a lack of turbostratic defects. The latter of which is
209 characteristic of smectitic interlayers.
210 Typical SAED patterns for each sample are presented in Figure 5. Chochołów-06 is the only
211 sample that deviates from the hexagonal single crystal diffraction patterns observed for
212 Chochołów-60, Bukowina Tatrzańska-06 and Bukowina Tatrzańska-41. Chochołów-06 has a
213 well-defined coherence of layers in its mixed-layer crystal particle with varying orientations of

these particles around c* (or Z) producing a slight ring effect, However, one mixed-layer crystal is thick enough to define the dominant single crystal pattern.

4.2 High resolution TEM imaging

Lattice fringe images of illite and illite-smectite in samples from Bukowina Tatrzańska-06 and Bukowina Tatrzańska-41 are presented in Figure 6. Bukowina Tatrzańska-06 shows thin illite packets which, based on a 10Å lattice spacing, are typically around 5 layers and are situated adjacent to I-S packets of similar thickness. Some I-S mixed layers show some lattice defects such as layer terminations (Figure 6a), whilst others are straight crystals (Figure 6b). In comparison, the samples from Bukowina Tatrzańska-41 typically reveal thicker I-S particles of 10-15 layers (Figure 6c and d). Here, some diagenetic crystallite packets are terminated against thick illite minerals of, presumably, detrital origin. I-S crystallites show some edge dislocations defined by terminations of layers of illite, probably inherited from highly imperfect, smectite precursor structures. In general, the samples in Figure 6 show substantial I-S growing adjacent to authigenic and detrital illite minerals. These I-S mixed layers display variable lattice morphologies with some collapse structures, detailing the probable prior existence of an expandable smectite component.

4.3 Chemistry

Bulk mineralogical data from Chochołów PIG-1 and Bukowina Tatrzańska PIG-1 is synthesized from Środoń et al. (2006b) and Day-Stirrat et al. (2008a) (Table 1). Standard structural formulae for an illite-smectite half-cell and associated elemental concentrations expressed as weight percent oxides are presented in Tables 2 to 5 for Chochołów-06, Chochołów-60, Bukowina Tatrzańska-06, Bukowina Tatrzańska-41, respectively. Both the octahedral totals (range = 1.92 to

238 2.11) and the chemical compositions are within the previously published range for illite-smectite;
239 some K^+ values are outside the range of illite, and even muscovite (>1), and are, therefore,
240 unrealistic and probably related to the noted mobility of potassium under an electron beam (Ahn
241 and Peacor, 1986; Brusewitz, 1986; Ramseyer and Boles, 1986; Środoń et al., 1986; van der Pluijm
242 et al., 1988; Weaver, 1989; Jiang et al., 1990; Li et al., 1997; Hover et al., 1999; Masuda et al.,
243 2001). The Si:Al ratio in the tetrahedral sheet is consistent with illitic material rather than pure
244 mica (Figure 7).

245 In order to compare the chemical composition of I-S from Chochołów-06 (50% I in I-S)
246 with that of the other samples (all 76% I in I-S), the Kolmogorov-Smirnov test is employed as
247 there are not enough data to adequately define averages by arithmetic means. Chochołów-06 has
248 a broader range of tetrahedral Si^{4+} values but includes values which are similar to or lower than
249 those in the more illitic I-S from Chochołów-60 (Figure 8a). Gulf Coast data previously published
250 by Ahn and Peacor (1986a) are presented as a reference frame for progressive illitization and
251 demonstrate the utility of the K-S test; however, it should be noted that these samples are not an
252 analog for the Podhale Basin.

253 The octahedral cation chemistry (Figure 8b and 8c) of Chochołów-06 displays a similar
254 range to that in the more illitic samples from Chochołów-60, albeit with more samples relatively
255 enriched in Fe^{3+} and Mg^{2+}. Total Al^{3+} is reflective of tetrahedral Si^{4+} occupancy and octahedral
256 substitution. The relative difference between sample data is described as a D-Statistic in Table 6.

257 I-S from Bukowina Tatrzańska-41 has a more homogeneous tetrahedral composition and a
258 much more aluminous octahedral composition than Bukowina Tatrzańska-06, which is richer in
259 Fe^{3+} (calculated Kolmogorov-Smirnov D-statistic of 43%; Figure 8f). Furthermore, the octahedral
260 composition of I-S in Bukowina Tatrzańska-41 is much more homogeneous than that in Bukowina
261 Tatrzańska-06. The D-statistic shows that all samples analyzed are statistically different in terms

of their octahedral cation compositions. The distributions (Figure 8) and the D-statistics (Table 6) show that Bukowina Tatrzańska-41 has less Fe^{3+} and Mg^{2+} and more Al^{3+} in its octahedral sites than Bukowina Tatrzańska-06.

5. Discussion

The composition of I-S reflects both that of the initial detrital supply and also changes resulting from diagenesis, which ultimately transform I-S to illite, and perhaps chlorite and quartz (Hower et al., 1976; Boles and Franks, 1979; Weaver, 1989; van de Kamp, 2008). From a general chemical perspective, the illitization of smectite results in the export of Fe^{3+} (or Fe^{2+}) and Mg^{2+} from I-S to chlorite or perhaps late-diagenetic ankerite, an increase in the concentration of Al^{3+} within illite, and the formation of quartz as the more siliceous smectite is converted to illite. It is commonly understood that Al^{3+} is conserved (Land et al., 1997; Land and Milliken, 2000) within a diagenetic system. Whilst these general trends are well documented, they may be masked in a single case by natural variations in the composition of detrital I-S related to provenance changes. A common provenance and well-documented, progressive and predictable diagenetic trends (Środoń et al., 2006b) makes this dataset from Podhale Basin ideal for high resolution study. Furthermore, illitization of smectite has been documented to play an important role on the development of an oriented alignment of neoformed clay minerals (Day-Stirrat et al., 2008a) in the Podhale Basin.

The chemical and mineralogical data presented here show that in the deeper parts of the basin (5000m to 7000m of maximum burial) the rate of smectite illitization has slowed or terminated, such that the % I in I-S does not change further (Table 1). Nevertheless, detailed analysis of I-S chemistry (Figure 6) and morphology (Figure 8) suggests continued recrystallization with increasing depth, observed as an increase in the size and coherency of I-S

crystallite packets. In terms of the use of sonic velocity as a method to estimate porosity and pore pressure, the implication of increased preferred orientation and thicker, more coherent I-S packets is increased velocities at a constant porosity and pore fluid pressure.

Further, with increasing burial depth, K_2O in the whole rock (Środoń et al., 2006b) is approximately conserved (Table 1). By assuming that K-feldspar contains 15% K^+ in its structural formula (i.e. 0.1 Na per formula: Środoń, 2009) and assigning an appropriate percentage of the K_2O to K-feldspar, the rest of the K_2O can be assigned to K-bearing 2:1 clays (mica, illite and illite-smectite; Table 1). These calculations show that the K_2O content of the 2:1 clay fraction does not evolve down the profile, staying between 5.6 and 7.4%. This consistency, despite a clear smectite illitization trend, can be explained only by a redistribution of K_2O within the 2:1 fraction (dissolution of detrital illite/mica providing K_2O for neoformed illite). Dissolution of illite with increasing burial depth is probably unreasonable as illite would be in equilibrium with smectite illitization.

It is well known that smectite produces concentric ring patterns in SAED associated with turbostratic disorder (Moore and Reynolds, 1997), resulting from the weak mutual attraction between hydrated cations in the interlayer space and adjacent 2:1 layers and the resultant lack of 'keying' effects which allows more random layer positioning. XRD indicates that the most diagenetically immature sample in this study contains randomly interstratified (R0) I-S with 50% illite layers (Środoń et al., 2006b), but only limited turbostratic disorder (Figure 5). The nature of the smectite and illite interfaces in interstratified mixed-layered 'crystallite packets' can affect SAED patterns (Bell, 1986), as the boundary between smectite and illite layers may be layer terminating, changing the crystal lattice planes on the scale of the electron beam and producing what appears to be small amounts of turbostratic disorder (see Figure 5). The three more diagenetically mature samples contain R1 ordered I-S (Środoń et al., 2006b) with essentially

identical (76%) proportions of I in I-S; these samples have correspondingly similar SAED patterns which are also similar to those observed in previous studies of similar material (e.g. Ahn and Peacor, 1986; Jiang et al., 1990). However, the ordering suggested by XRD is not entirely matched by the high resolution TEM observations, which show progressive ordering from Bukowina Tatrzańska-06 to Bukowina Tatrzańska-41 and an increase in crystallite size. This suggests that I-S continues to recrystallize beyond the level implied by XRD data, revealed by TEM because this technique can discern a packet of crystallites within a size fraction, whereas XRD is the average crystallographic response of all the crystallites in that fraction. Small differences in SAED patterns of the three more mature samples most probably relate to (a) the coherency of 'crystallite packets', with larger packets producing more clearly identified single crystal patterns (Ahn and Peacor, 1986; Li et al., 1997), and (b) the octahedral substitution of Fe^{3+} (or Fe^{2+}) and Mg^{2+} for Al^{3+} in the octahedral layer, with Fe^{3+} being the most significant substitution due to the size of the atom relative to Al^{3+}. The most coherent SAED patterns for I-S are thus seen in Bukowina Tatrzańska-41, which contain, according to lattice fringe images (Figure 6), the thickest I-S crystallites which also have the least Fe^{3+} and Mg^{2+} in the octahedral sheet (Figure 8).

It has been previously shown that on a $1mm^2$ scale, the preferred orientation of I-S crystallites (Figure 2) in these wells increases substantially during the main phase of illitization (Day-Stirrat et al., 2008a); a similar phenomenon was observed in the Gulf of Mexico by Ho et al. (1999). The change in preferred orientation implies that illitization occurs as a dissolution – reprecipitation reaction and that the neoformed mineral grows perpendicular to maximum effective stress (Day-Stirrat et al., 2008a). In the closed system implied by the whole rock chemistry (constant K_2O) and mineralogy of these mudstones (Środoń et al., 2006b), potassium for illite is supplied from K-feldspar, with additional Al^{3+} and Si^{4+} from kaolinite. Changes in the proportion of illite in mixed-layer I-S halt at around 5 km paleo burial depth that is around 100°C

(Table 1, Figure 2). More deeply buried samples, such as Bukowina Tatrzańska-41, which has a maximum burial depth of 7.1 km and a maximum paleo-temperature of close to 150°C (Środoń et al., 2006a), have essentially identical % I in I-S. However, in the apparent absence of % I in I-S change, the preferred orientation of I-S in the more deeply buried samples is somewhat higher. These data could imply (a) mechanical rearrangement of phyllosilicates as a result of higher effective stresses; (b) continued recrystallization but with no change in % I within I-S; (c) formation of a variably aligned phyllosilicate fabric during the main phase of illitization, with no further recrystallisation during continued burial.

It is highly unlikely that the somewhat enhanced preferred orientation is due to mechanical rearrangement. Firstly, the samples have low porosities and secondly, mercury injection porosimetry data suggest that most pores are smaller than ~ 20 nm (Day-Stirrat et al., 2008a). The lack of physical space precludes substantial mechanical reorientation of particles which are larger than the pores. Given that the diagenetic system here appears to be closed, any change in the microfabric is likely to result in a shift of load from matrix grains to pore fluid,a decrease in effective stress, an argument recently discussed by Goulty et al. (2016). Given that the pore volume to matrix volume is weighed heavily in favor of the matrix, any change could have proportionally large effects on pore fluid. Therefore, in high pressure high temperature wells the loading-unloading behavior (Bowers, 1995), decrease in effective stress, may be extremely complex and potentially away from illite compaction trends defined for lower effective stresses (Lahann, 2002; Lahann and Swarbrick, 2011).

Unfortunately, our data cannot unequivocally differentiate hypotheses (b) and (c). However, lattice fringe images suggest that I-S crystallite packages in Bukowina Tatrzańska-41 are larger than those in Bukowina Tatrzańska-06, implying continuing crystal growth without the destruction of smectite layers in mixed-layer I-S (Figure 6). We infer that the I-S does not

358 become more illitic due to a lack of supply of K^+, or that residual smectite layers are physically
359 occluded from interacting with cations in solution. A clear compositional difference (Figure 8)
360 between I-S in Bukowina Tatrzańska-06 and Bukowina Tatrzańska-41 supports the idea of
361 continued recrystallization. The octahedral occupancy of I-S in Bukowina Tatrzańska-41 is much
362 more aluminous than that of Bukowina Tatrzańska-06, essentially more mica like, and the
363 overall composition of I-S in Bukowina Tatrzańska-41 is much more homogeneous than that in
364 Bukowina Tatrzańska-06. Stated very simply, Bukowina Tatrzańska-41 has a distribution of
365 illite-smectite chemical formulae that are simplified relative to Bukowina Tatrzańska-06,
366 consistent with the progressive conversion of illite towards a 'mica' at significantly greater
367 temperatures (van de Kamp, 2008).
368 The data in this study, plus those from Środoń et al. (2006b) and Day-Stirrat et al.
369 (2008a), indicate continued recrystallization and export of Fe^{3+} from I-S as, during late
370 diagenesis, it transforms towards a more muscovite-like composition. We propose that this is
371 part of a series of diagenetic steps (Figure 9) that converts a broadly isotropic fabric inherited as
372 a result of the deposition of clay floccules to the highly aligned fabric observed in low grade
373 metamorphic pelites (Haines et al., 2009). Reorientation of the clay fabric is restricted during the
374 main stage of mechanical compaction, during which water is expelled, but is enhanced during the
375 main stage of smectite illitization. In this study, at higher levels of diagenesis, we see that whilst
376 recrystallization of illite continues, there is a limited change in the orientation of the illite fabric.
377 As diagenesis gives way to low grade metamorphism, there is once again a more striking
378 development of an aligned phyllosilicate fabric, reflecting continuing clay mineral
379 recrystallization and growth (Figure 9). Abrupt diagenetic steps are not applicable to all major
380 diagenetic reactions. For example, once quartz cementation reaches a kinetically favorable

activation energy (with the presence of a clean quartz surface) and temperature the reaction simply runs until there is no more space for quartz cementation (Taylor et al., 2010).

6. Conclusions

TEM-EDS data and statistical tests presented here describe a systematic change in I-S chemistry with increased burial temperature beyond the termination of the smectite to illite transformation. TEM-EDS data is accompanied by SAED patterns that show well defined coherence of layers in I-S packets, single crystal patterns and an absence of turbostratic disorder. Concomitant with this change in mineral formulae is an increase in crystallinity observable in lattice fringe images and a change from high angle contacts between discrete I-S packets to more coalesced crystallites. We propose that the data presented here describe the continued increase in the preferred orientation of I-S beyond the smectite to illite transformation. This involves a change in crystallite chemistry reflected by (a) the progressive removal of Fe^{3+} and Mg^{2+} from the octahedral sheet of I-S, (b) a decrease in crystallite layer rotation and (c) the coalescence of I-S crystallites in a high effective stress regime. We suggest that these relatively subtle changes are one of a series of diagenetic steps which convert chemically diverse I-S with a broadly isotropic phyllosilicate fabric into chemically homogeneous illite with a highly anisotropic fabric in low grade metamorphic rocks. These results have implications for loading-unloading trends in diagenetically mature siliciclastic systems and for predicating porosity and pore pressure from wireline logs.

7. Acknowledgements

We thank the UK Natural Environment Research Council (NERC) and BP for supporting RJD-S's PhD which generated the TEM-EDS data and the EMAL at the University of Michigan for use of their TEM and sample preparation equipment for lattice fringe imaging.

Table 1 Present day depth [m], maximum burial depth [m], %I in I-S and bulk mineralogy from X-ray diffraction (Środoń et al., 2006b).

Sample	ChI-4	ChI-6	ChI-12	ChI-20	ChI-23	ChI-28	ChI-38	ChI-44	ChI-56	ChI-60	ChI-66
Actual Burial Depth (m)	193	280	514	821	1031	1283	1671	2012	2410	2611	2968
Estimated Maximum Burial Depth [m]	2393	2480	2714	3021	3231	3483	3871	4212	4610	4811	5168
Max. Temp (°C) from modeling	57.5	60	67.5	75	80	85	95	105	115	120	127.5
Quartz	19.0	24.3	18.5	22.9	21.7	20.4	16.3	26.0	20.5	27.5	22.4
K-Feldspar	2.2	2.3	2.2	1.5	1.3	0.5	1.5	1.0	0.5	0.4	0.5
Plagioclase	3.0	5.9	3.7	4.7	3.6	5.7	5.0	7.0	6.5	9.0	6.0
Calcite	7.7	10.2	11.9	10.5	10.0	10.4	0.9	3.7	3.6	13.2	17.0
Dolomite	3.8	5.4	3.5	4.1	4.5	4.7	4.5	6.2	5.2	4.6	6.7
Halite	0.0	0.0	0.0	0.0	0.0	0.0	0.6	0.5	1.2	0.0	0.0
Pyrite	1.5	1.5	1.2	0.7	0.9	2.3	2.3	2.5	1.8	1.2	1.5
Siderite	0.0	0.4	0.3	0.7	0.8	0.0	0.0	0.2	0.0	0.2	0.2
Anatase	0.0	0.0	0.0	0.0	0.2	0.0	0.6	0.4	0.5	0.7	0.5
Kaolinite	3.2	1.5	3.2	3.6	2.9	2.6	1.0	1.0	0.8	0.0	0.0
Illite + Mica + Fe-Smectite	45.8	46.8	50.2	49.2	43.9	49.1	60.8	53.9	60.1	41.1	41.8
Chlorite	0.7	4.0	2.6	2.1	2.6	3.6	7.4	5.2	4.8	4.7	4.2
Total clay	49.7	52.3	56.0	54.9	49.4	55.3	69.2	60.1	65.7	45.8	46.0
%S in I/S	52	50	63	47	45	44	24	32	27	24	31
Ordering	0	0	0	0	0/1	0/1	1	1	1	1	1
K2O (%)	3.6	3.6	3.2	3.0	2.9	3.0	4.7	3.4	4.2	2.9	2.9
K-Bearing 2:1 clays	22.0	23.4	18.6	26.1	24.1	27.5	46.2	36.7	43.9	31.2	28.8
K_2O in Illite Wt.%	2.4	2.3	2.2	2.3	2.3	2.8	3.6	2.9	3.9	2.7	2.7
% K_2O in Illite	9.1	10.0	8.6	11.4	10.3	9.9	12.7	12.7	11.2	11.5	10.8
K_2O/K-Feldspar	1.6	1.5	1.5	2.0	2.2	6.0	3.1	3.4	8.5	7.3	5.8
TEM Study Samples And %I in I-S		ChI-6 50%								ChI-60 76%	

Sample	BkT-1	BkT-6	BkT-12	BkT-17	BkT-23	BkT-28	BkT-35	BkT-41
Actual Burial Depth (m)	102	294	611	903	1261	1595	1904	2201
Estimated Maximum Burial Depth [m]	4908	5100	5417	5709	6067	6401	6710	7007
Max. Temp (°C) from modeling	103	107	114	120	127	134	141	147
Quartz	26.6	25.2	27.0	24.1	23.3	27.0	29.4	26.4
K-Feldspar	0.8	0.5	1.0	0.5	1.0	0.0	0.5	0.0
Plagioclase	7.1	6.8	6.6	5.3	4.5	6.2	6.3	5.7
Calcite	9.5	7.3	5.4	6.9	6.1	11.2	0.8	8.8
Dolomite	7.5	6.5	7.6	6.9	7.8	5.5	6.2	4.2
Halite	0.0	0.0	0.0	0.5	0.0	0.0	0.5	1.0
Pyrite	0.9	0.9	1.2	1.3	1.0	1.5	2.4	3.0
Siderite	0.0	0.5	0.0	0.0	0.0	0.0	0.0	0.0
Anatase	0.5	0.5	0.5	0.5	0.4	0.4	0.5	0.3
Kaolinite	0.8	0.5	0.0	0.0	0.0	0.0	0.0	0.0
Illite + Mica + Fe-Smectite	53.6	54.3	52.0	48.1	50.7	46.8	50.1	51.5
Chlorite	5.6	5.6	6.1	3.1	4.2	4.4	3.6	4.0
Total clay	60.0	60.4	58.1	51.2	54.9	51.2	53.7	55.5
%S in I/S	25	24	26	25	20	30	18	24
Ordering	1	1	1	1	1	1	1	1
K_2O (%)	3.5	3.6	3.1	3.3	3.3	3.1	3.4	3.3
K-Bearing 2:1 clays	40.2	41.3	38.5	36.1	40.6	32.8	41.1	39.1
K_2O in Illite Wt.%	3.1	3.3	2.6	3.1	2.8	3.1	3.1	3.3
% K2O in Illite	13.1	12.6	14.6	11.8	14.5	10.6	13.1	11.9
K_2O/K-Feldspar	4.4	7.1	3.1	6.6	3.3		6.8	
TEM Study Samples And %I in I-S		BkT-6 76%						BkT-41 76%

Table 2: Chochołów-06 structural formulae for a half cell and associated elemental concentrations expressed as wt.% oxides normalized to 95%.(Merriman et al., 1995), 50 % illite in illite-smectite.

	E001	*E003*	*E005*	*E009*	*E011*	*E019*
Si	3.31	3.65	3.12	3.56	3.12	3.59
Al	0.69	0.35	0.88	0.44	0.88	0.41
Tet. Sum	4.00	4.00	4.00	4.00	4.00	4.00
Al	1.93	1.77	1.47	1.59	1.73	1.61
Fe	0.07	0.07	0.20	0.14	0.07	0.15
Mg	0.00	0.10	0.23	0.28	0.19	0.20
Ti	0.01	0.02	0.02	0.00	0.03	0.00
Oct. Sum	2.01	1.96	1.92	2.01	2.02	1.96
Ca	0.00	0.02	0.00	0.02	0.01	0.03
K	0.68	0.52	1.34	0.66	0.95	0.67
Inter. Sum	0.68	0.54	1.34	0.68	0.96	0.70
SiO_2	50.24	57.21	44.78	54.52	46.67	0.69
Al_2O_3	33.77	28.18	28.50	26.23	33.08	33.08
TiO_2	0.17	0.47	0.41	0.35	0.69	0.15
Fe_2O_3	1.37	1.46	3.72	2.88	1.37	11.15
MgO	1.24	1.01	2.24	2.88	1.88	46.67
CaO	0.16	0.24	0.33	0.28	0.15	1.88
K_2O	8.05	6.43	15.04	7.86	11.15	1.37
Total	95	95	95	95	95	95
	E021	*E024*	*E026*	*E028*	*E030*	
Si	3.50	3.44	3.32	3.26	3.04	
Al	0.50	0.56	0.68	0.74	0.96	
Tet. Sum	4.00	4.00	4.00	4.00	4.00	
Al	1.48	1.63	1.62	1.69	1.55	
Fe	0.24	0.18	0.15	0.19	0.20	
Mg	0.25	0.16	0.14	0.09	0.33	
Ti	0.03	0.02	0.01	0.03	0.02	
Oct. Sum	2.00	1.99	1.92	2.00	2.10	
Ca	0.19	0.02	0.25	0.01	0.09	
K	0.34	0.66	0.55	0.76	0.82	
Inter. Sum	0.53	0.68	0.80	0.77	0.91	
SiO_2	54.05	52.54	50.58	49.26	45.07	
Al_2O_3	25.88	28.45	29.69	31.16	31.59	
TiO_2	0.63	0.49	0.15	0.59	0.36	
Fe_2O_3	5.02	3.64	3.12	3.89	3.85	
MgO	2.57	1.62	1.39	0.92	3.27	
CaO	2.72	0.34	3.54	0.16	1.31	
K_2O	4.14	7.91	6.53	9.02	9.56	
Total	95	95	95	95	95	

Table 3: Chochołów-60 structural formulae for a half cell and associated elemental concentrations expressed as wt.% oxides normalized to 95%.(Merriman et al., 1995), 76 % illite in illite-smectite.

	J001	*J009*	*J011*	*J013*	*J015*	*J017*	*J019*	*J021*
Si	3.32	3.28	3.47	3.37	3.25	3.12	3.19	3.37
Al	0.68	0.72	0.53	0.63	0.75	0.88	0.81	0.63
Tet. Sum	4.00	4.00	4.00	4.00	4.00	4.00	4.00	4.00
Al	1.81	1.78	1.53	1.80	1.67	1.45	1.72	1.93
Fe	0.10	0.14	0.17	0.08	0.16	0.21	0.17	0.10
Mg	0.14	0.07	0.21	0.05	0.10	0.31	0.01	0.01
Ti	0.02	0.01	0.03	0.01	0.05	0.02	0.02	0.01
Oct. Sum	2.07	2.00	1.94	1.94	1.98	1.99	1.92	2.05
Ca	0.05	0.07	0.11	0.07	0.06	0.05	0.09	0.04
K	0.49	0.62	0.65	0.70	0.76	1.13	0.89	0.45
Inter. Sum	0.54	0.69	0.76	0.77	0.82	1.18	0.98	0.49
SiO_2	51.62	50.26	52.81	51.63	49.02	45.41	47.59	52.78
Al_2O_3	32.71	32.45	26.64	31.63	31.04	28.69	32.11	33.99
TiO_2	0.48	0.23	0.62	0.26	0.92	0.33	0.32	0.12
Fe_2O_3	2.00	2.94	3.42	1.59	3.16	3.99	3.28	2.05
MgO	1.48	0.76	2.19	0.53	1.00	3.07	0.08	0.06
CaO	0.77	0.95	1.54	0.96	0.84	0.67	1.20	0.52
K_2O	5.94	7.42	7.79	8.41	9.02	12.84	10.42	5.48
Total	95	95	95	95	95	95	95	95

445 Table 4: Bukowina Tatrzańska-06 structural formulae for a half cell and associated elemental concentrations expressed
446 as wt.% oxides normalized to 95%.(Merriman et al., 1995), 76 % illite in illite-smectite.

	H003	*H007*	*H009*	*H011*	*H013*	*H018*	*H022*
Si	3.36	3.22	3.38	3.52	3.32	3.42	3.26
Al	0.64	0.78	0.62	0.48	0.68	0.58	0.74
Tet. Sum	4.00	4.00	4.00	4.00	4.00	4.00	4.00
Al	1.66	1.32	1.68	1.66	1.76	1.76	1.72
Fe	0.20	0.34	0.18	0.12	0.14	0.07	0.14
Mg	0.22	0.28	0.03	0.16	0.07	0.17	0.05
Ti	0.00	0.02	0.01	0.00	0.01	0.01	0.01
Oct. Sum	2.08	1.96	1.90	1.94	1.98	2.01	1.92
Ca	0.19	0.00	0.03	0.04	0.00	0.01	0.06
K	0.22	1.18	0.91	0.73	0.80	0.71	0.89
Inter. Sum	0.41	1.18	0.94	0.77	0.80	0.72	0.95
SiO_2	52.40	46.43	50.66	53.39	50.30	52.61	48.84
Al_2O_3	30.52	25.62	29.21	27.60	31.49	30.38	31.35
TiO_2	0.03	0.32	0.16	0.53	0.21	0.25	0.28
Fe_2O_3	4.19	6.50	3.54	2.50	2.76	1.34	2.84
MgO	2.31	2.70	0.30	1.61	0.71	1.73	0.49
CaO	2.81	0.04	0.41	0.63	0.01	0.14	0.78
K_2O	2.75	13.39	10.71	8.75	9.51	8.55	10.42
Total	95	95	95	95	95	95	95
	H024	*H026*	*H028*	*H030*	*H032*	*H034*	
Si	3.17	3.39	3.07	3.39	3.10	3.46	
Al	0.83	0.61	0.93	0.61	0.90	0.54	
Tet. Sum	4.00	4.00	4.00	4.00	4.00	4.00	
Al	1.49	1.54	1.04	1.58	1.44	1.53	
Fe	0.22	0.26	0.56	0.19	0.22	0.15	
Mg	0.24	0.15	0.29	0.16	0.31	0.23	
Ti	0.00	0.05	0.06	0.02	0.05	0.02	
Oct. Sum	1.95	2.00	1.95	1.95	2.02	1.93	
Ca	0.10	0.07	0.22	0.01	0.04	0.00	
K	1.01	0.55	0.89	0.90	1.02	0.94	
Inter. Sum	1.11	0.62	1.11	0.91	1.06	0.94	
SiO_2	46.54	51.70	43.80	50.73	45.44	51.93	
Al_2O_3	28.87	27.72	23.78	27.82	28.98	26.28	
TiO_2	0.00	1.08	1.05	0.36	0.97	0.43	
Fe_2O_3	4.28	5.36	10.67	3.88	4.34	2.94	
MgO	2.38	1.55	2.77	1.56	3.01	2.36	
CaO	1.30	0.96	2.95	0.14	0.53	0.07	
K_2O	11.63	6.63	9.98	10.52	11.72	10.99	
Total	95	95	95	95	95	95	

447

Table 5: Bukowina Tatrzańska-41 structural formulae for a half cell and associated elemental concentrations expressed as wt.% oxides normalized to 95% (Merriman et al., 1995). 76 % illite in illite-smectite.

	C003	*C005*	*C007*	*C010*	*C012*	*C014*	*C016*	*C018*
Si	3.28	3.24	3.22	3.52	3.38	3.28	3.47	3.40
Al	0.72	0.76	0.78	0.48	0.62	0.72	0.53	0.60
Tet. Sum	4.00	4.00	4.00	4.00	4.00	4.00	4.00	4.00
Al	1.77	1.88	1.94	1.50	1.76	1.79	1.58	1.62
Fe	0.11	0.04	0.07	0.07	0.10	0.09	0.17	0.14
Mg	0.19	0.00	0.10	0.35	0.18	0.02	0.13	0.19
Ti	0.01	0.01	0.00	0.07	0.02	0.01	0.03	0.03
Oct. Sum	2.08	1.93	2.11	1.99	2.06	1.91	1.91	1.98
Ca	0.00	0.10	0.03	0.16	0.00	0.00	0.02	0.00
K	0.67	0.75	0.47	0.45	0.58	0.97	0.86	0.82
Inter. Sum	0.67	0.85	0.50	0.61	0.58	0.97	0.88	0.82
SiO_2	49.83	49.19	50.14	54.44	52.31	49.30	52.21	51.39
Al_2O_3	32.18	34.07	35.93	26.10	31.27	31.95	27.07	28.55
TiO_2	0.19	0.26	0.11	1.41	0.35	0.23	0.66	0.69
Fe_2O_3	2.27	0.81	1.52	1.52	2.13	1.88	3.40	2.75
MgO	1.94	0.27	1.00	3.64	1.90	0.16	1.27	1.91
CaO	0.63	1.43	0.50	2.38	0.05	0.02	0.23	0.01
K_2O	7.96	8.97	5.79	5.52	6.99	11.45	10.17	9.69
Total	95	95	95	95	95	95	95	95

Table 6. Summary of the difference using the Kolmogorov-Smirnov test between samples in the Podhale Basin (ND=no data).

Well and Sample	Difference in Fabric Intensity [m.r.d.]	Difference in % I in I-S	Difference in Octahedral Fe D-Statistic	Difference in Octahedral Mg D-Statistic	Difference in Total Al D-Statistic	Difference in Tetrahedral Si D-Statistic
20% I in I-S and 80% I in I-S (Ahn and Peacor, 1986)	ND	60	75	76	88	100
Chochołów-06 and Chochołów-60	1.48	26	45	40	28	30
Bukowina Tatrzańska-06 and Bukowina Tatrzańska-41	1.2	0	43	30	18	18
Chochołów-06 and Bukowina Tatrzańska-06	0.25	26	37	10	5	8
Chochołów-06 and Bukowina Tatrzańska-41	2.53	26	50	27	18	25
Chochołów-60 and Bukowina Tatrzańska-06	0.32	0	40	48	23	27
Chochołów-60 and Bukowina Tatrzańska-41	0.95	0	39	23	4	25

509

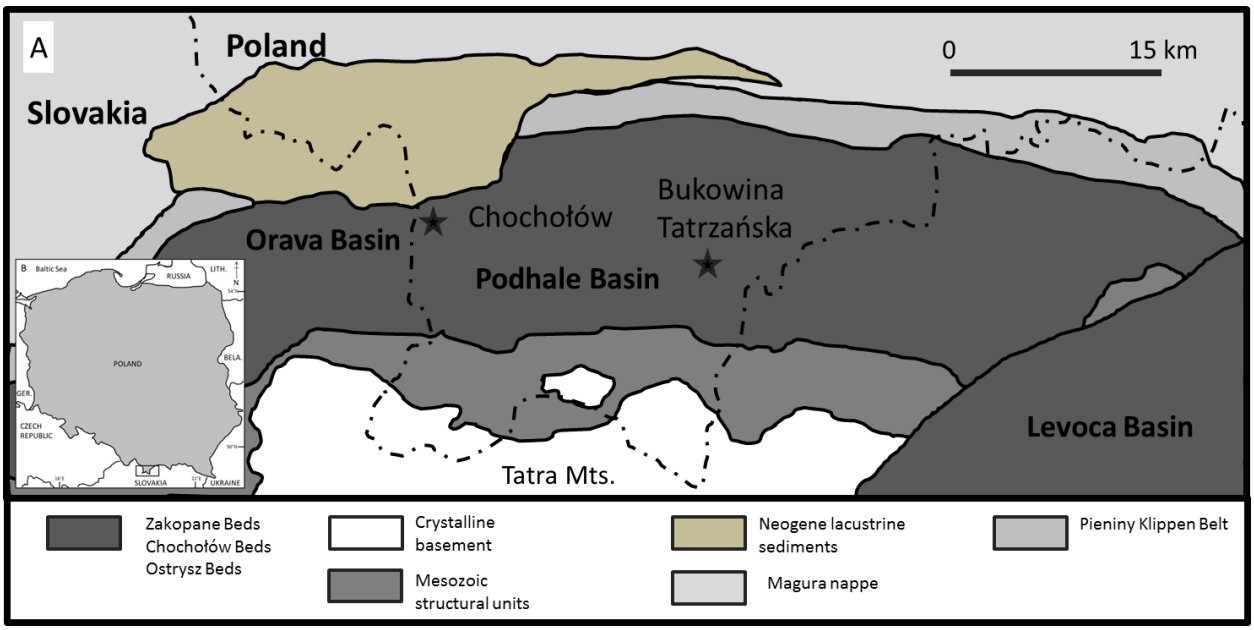

510

511 Figure 1. A: The Podhale Basin with its surrounding sub-basins. and the locations of the Chochołów PIG-1 and
512 Bukowina Tatrzańska PIG-1 wells (adapted from Środoń et al., 2006b).
513

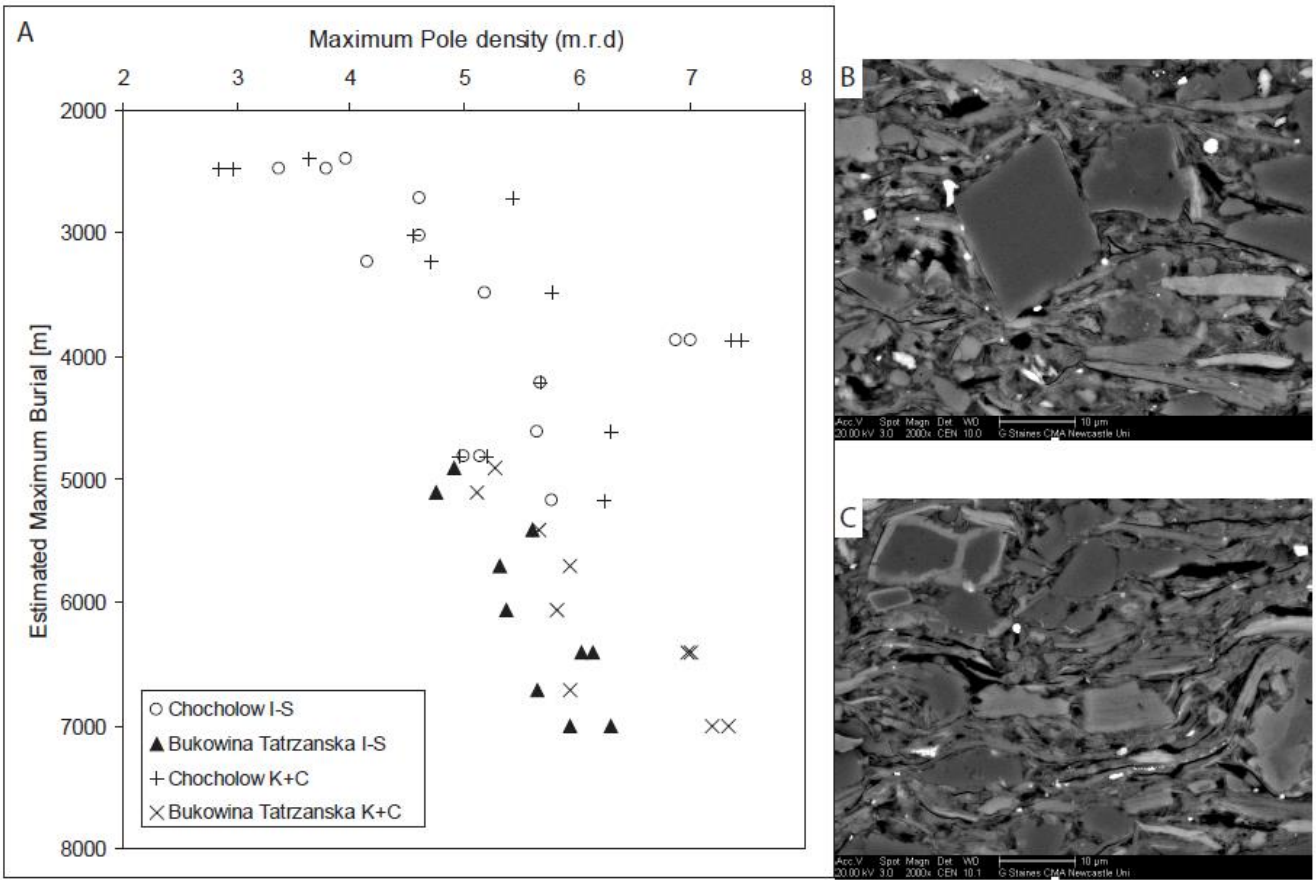

514
515 Figure 2. (A) Maximum pole density (m.r.d.) for illite-smectite and kaolinite + chlorite for samples from the Podhale
516 Basin (Day-Stirrat et al, 2008a). Backscattered electron images (B) and (C) of samples at 2480m and 4610m (see Day-
517 Stirrat et al, 2008a for more images). Smectite illitization appears to terminate at around 4500 m of maximum burial.

Figure 3. Sample Bukowina Tatrzańska-06 H013 (TEM-EDS data in Table 4). Euhedral grain drop-cast on a carbon film-supported 200-mesh copper grid with c* (Z) parallel to the electron beam. The scale bar is 200nm and the location of diffraction aperture is schematically noted by the ring. The Selected Area Diffraction Pattern (inset) shows a strong hexanet of discrete spots free from distortions or rings that are indicative of turbostratic layering.

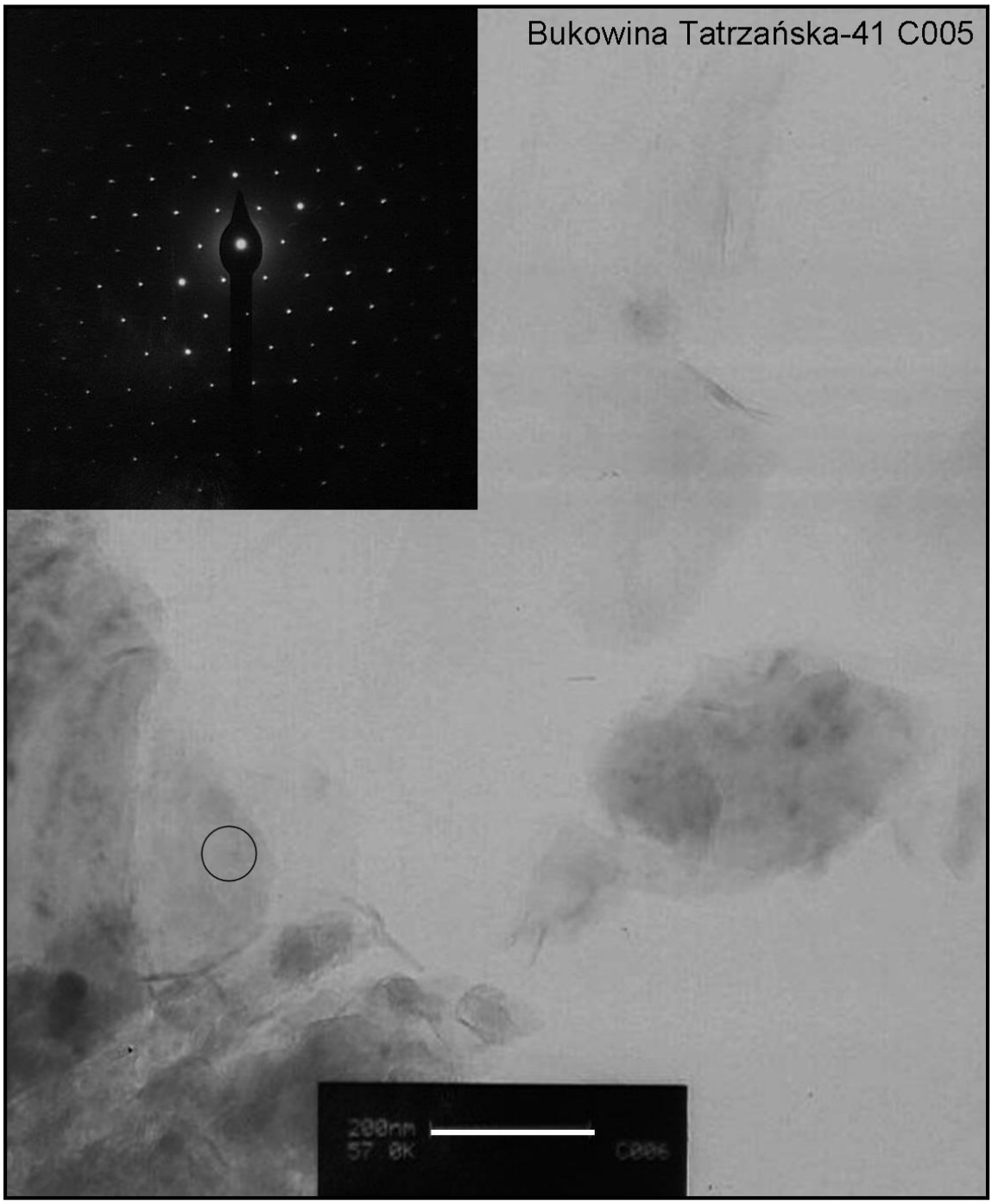

Figure 4. A grain in sample Bukowina Tatrzańska-41 C005 (TEM-EDS data in Table 5). Grain drop-cast on a carbon film-supported 200-mesh copper grid with c* (Z) parallel to the electron beam. The scale bar is 200nm and the location of diffraction aperture is schematically noted by the ring. The Selected Area Diffraction Pattern (inset) shows a strong hexanet of discrete spots free from distortions or rings that are indicative of turbostratic layering.

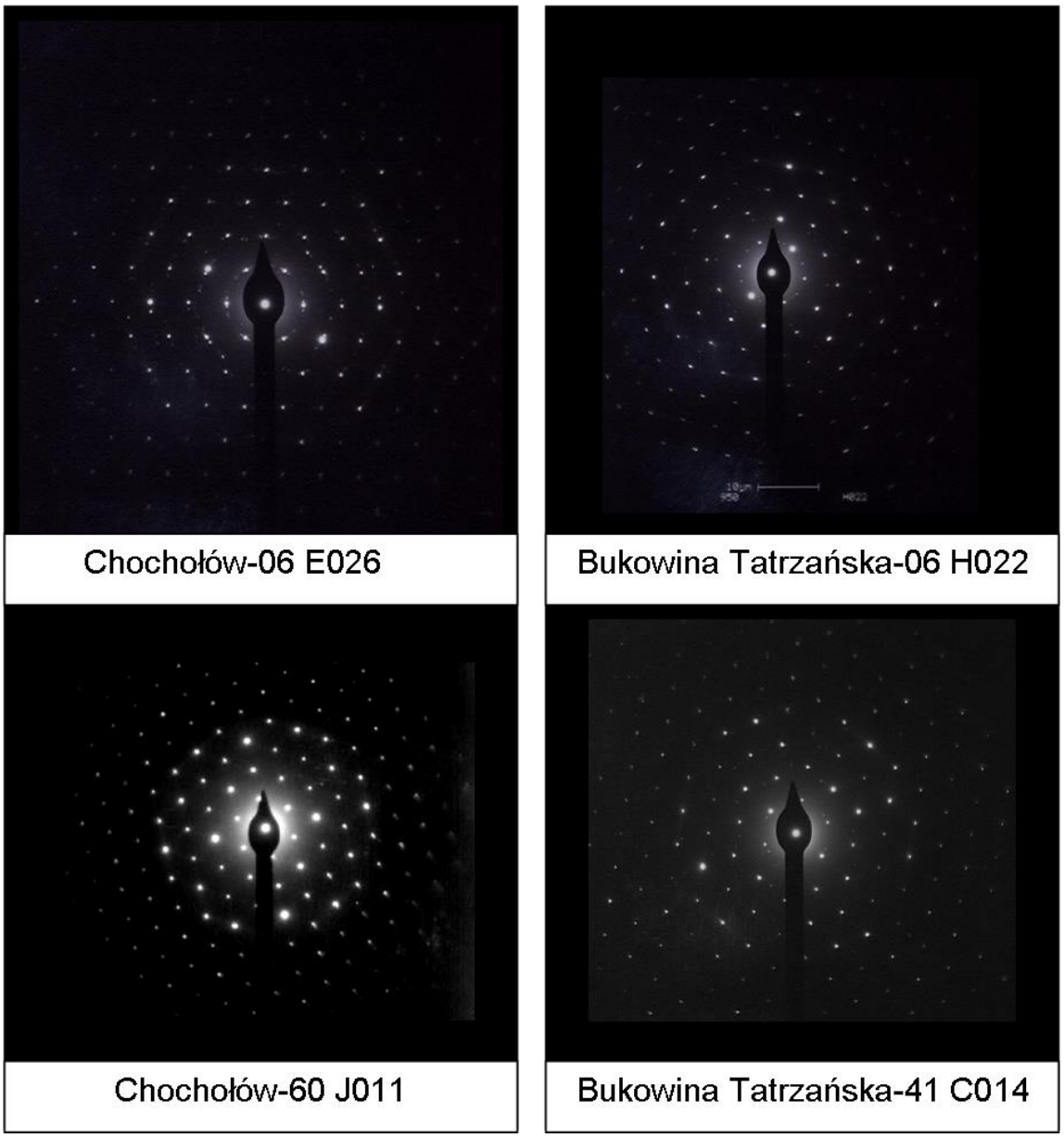

Figure 5. Representative Selected Area Diffraction Patterns for samples Chochołów-06, Chochołów-60, Bukowina Tatrzańska-06 and Bukowina Tatrzańska-41 (Tables 2, 3, 4 and 5 for mineral formulae). Chochołów-06 shows well defined coherence of layers in packets with varying orientations, but with one packet that is thick enough to produce a hexagonal single crystal pattern. Chochołów-60, Bukowina Tatrzańska-06 and Bukowina Tatrzańska-41 have Selected Area Diffraction Patterns for (*h,k,0*) showing well-defined single crystal patterns.

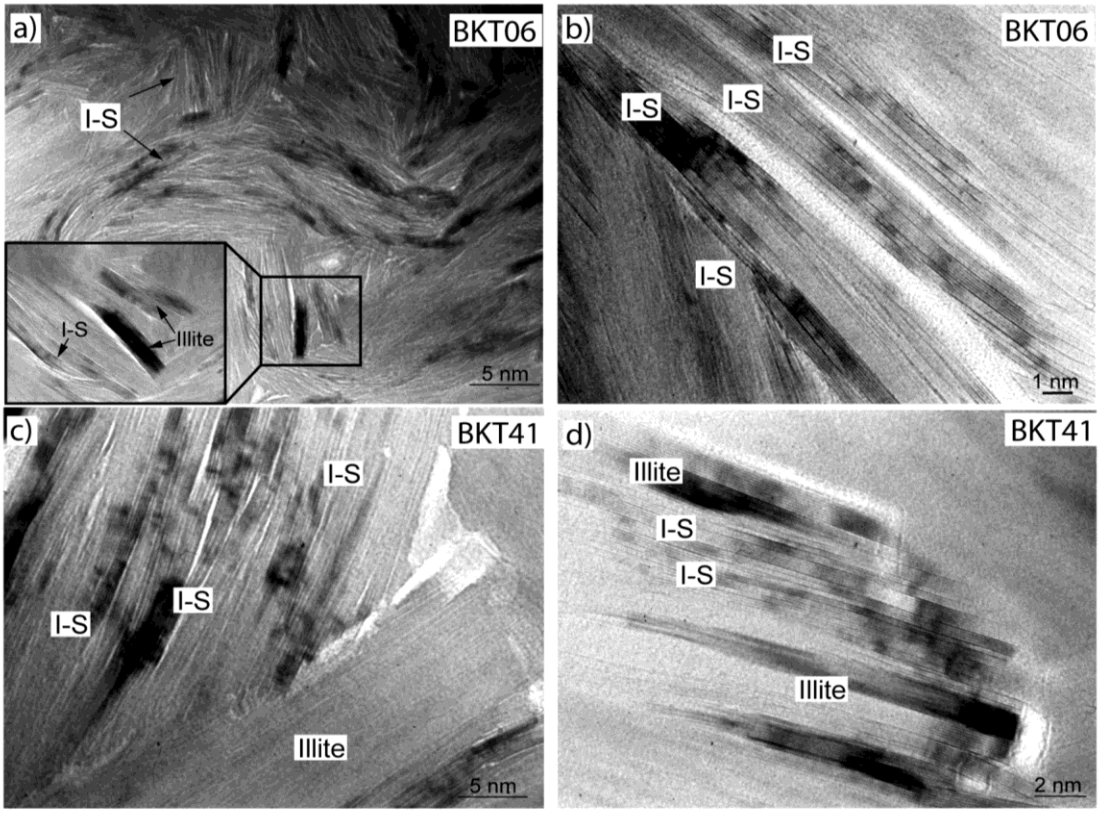

Figure 6. Lattice fringe images of samples Bukowina Tatrzańska-06 and Bukowina Tatrzańska-41 at varying magnifications. A) Thin illite packets growing within illite-smectite (I-S) layers, illite is not continuous with I-S. Layer terminations can be seen in the inset figure, where the arrow pointing to I-S lines on a layer termination B) I-S packets are not continuous and packets are oriented at large angles to each other, C) I-S packets terminate against a thick illite packet (detrital in origin), white areas separating I-S packets are probably indicative of smectite collapse and here may be viewed as porosity at the angstrom scale, D) illite growing within I-S layers, illite packets generally more coherent than I-S.

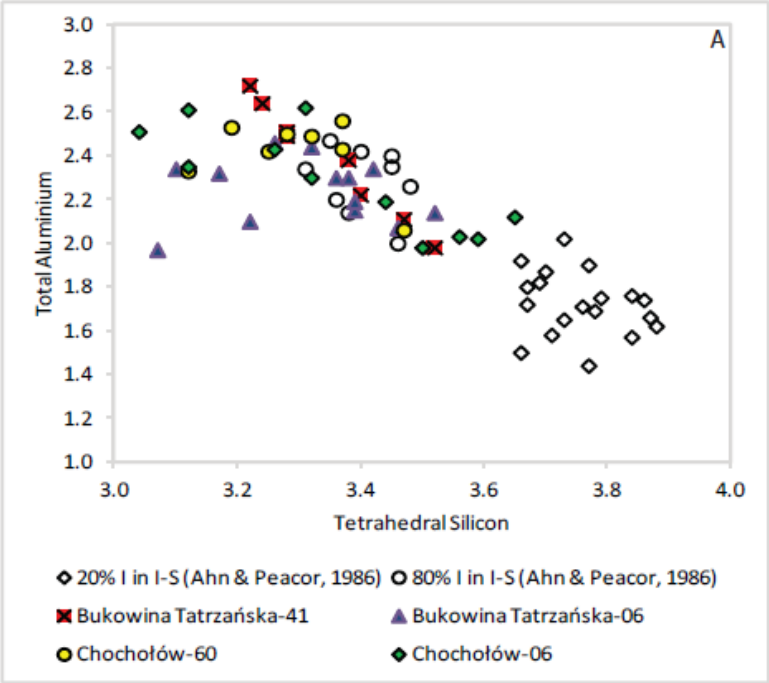
A
Total Aluminium
Tetrahedral Silicon
20% I in I-S (Ahn & Peacor, 1986)
80% I in I-S (Ahn & Peacor, 1986)
Bukowina Tatrzańska-41
Bukowina Tatrzańska-06
Chochołów-60
Chochołów-06

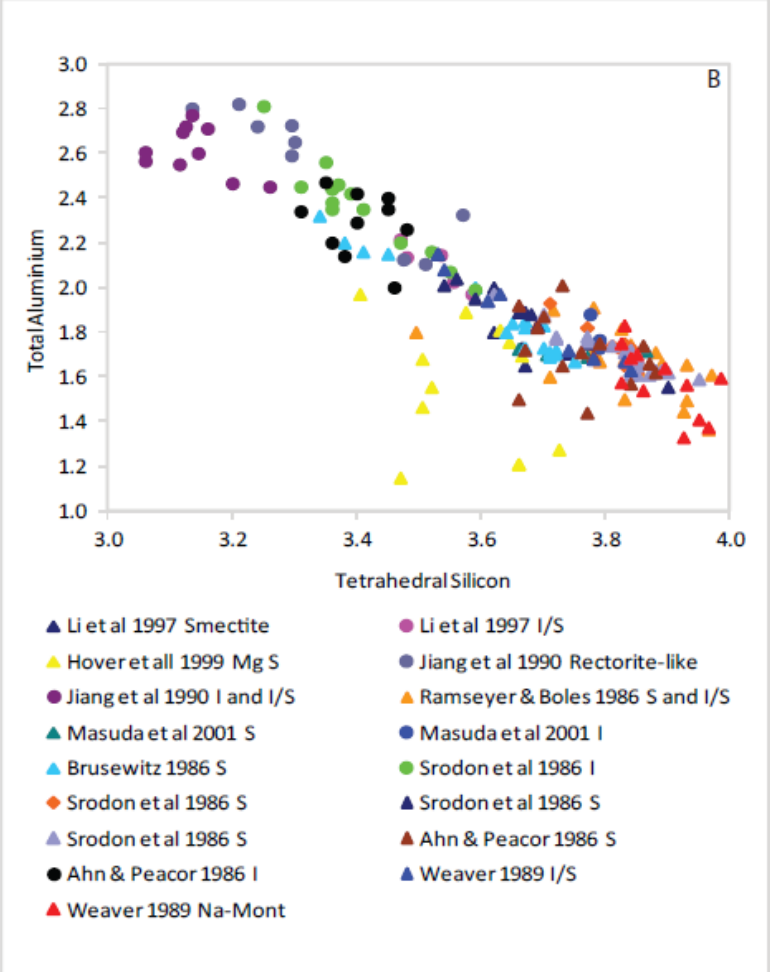
B
Total Aluminium
Tetrahedral Silicon
Li et al 1997 Smectite
Li et al 1997 I/S
Hover et all 1999 Mg S
Jiang et al 1990 Rectorite-like
Jiang et al 1990 I and I/S
Ramseyer & Boles 1986 S and I/S
Masuda et al 2001 S
Masuda et al 2001 I
Brusewitz 1986 S
Srodon et al 1986 I
Srodon et al 1986 S
Srodon et al 1986 S
Srodon et al 1986 S
Ahn & Peacor 1986 S
Ahn & Peacor 1986 I
Weaver 1989 I/S
Weaver 1989 Na-Mont

548

549 Figure 7. (A) Tetrahedral Si^{4+} versus total Al^{3+} for Chochołów-06, Chochołów-60, Bukowina Tatrzańska-06 and
550 Bukowina Tatrzańska-41 from TEM-EDS, data from Ahn and Peacor (1986a) are also shown. (B) Tetrahedral Si
551 versus total Al from the noted literature sources. Data are from a variety of techniques; Atomic absorption
552 Spectroscopy, DC Plasma-Emission Spectroscopy, Ignited weights, X-ray fluorescence and not TEM-EDS alone. The
553 division of the data into illite (I), illite-smectite (I/S), and smectite (S) is based on the individual author's descriptions.

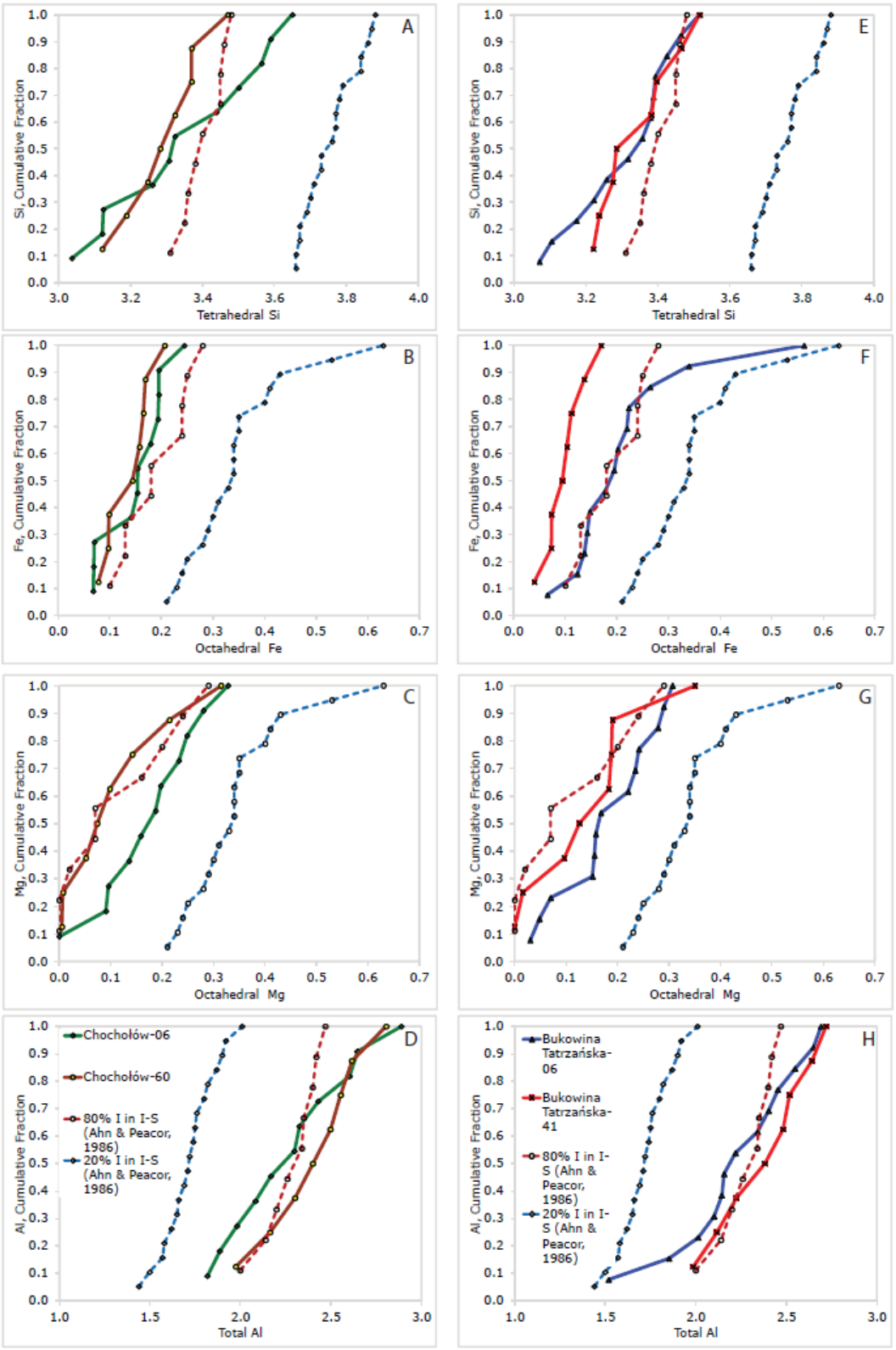

Figure 8. Kolmogorov-Smirnov distributions of (a,e) tetrahedral Si, (b,f) octahedral Fe, (c,g) octahedral Mg and (d,h) Total Al for comparisons of Chochołów-6 with Chochołów-60 and Bukowina Tatrzańska-06 with Bukowina Tatrzańska-41. Data from Ahn and Peacor (1986a) for the Texas Gulf Coast are also shown to show the separation of the data and, therefore, their difference.

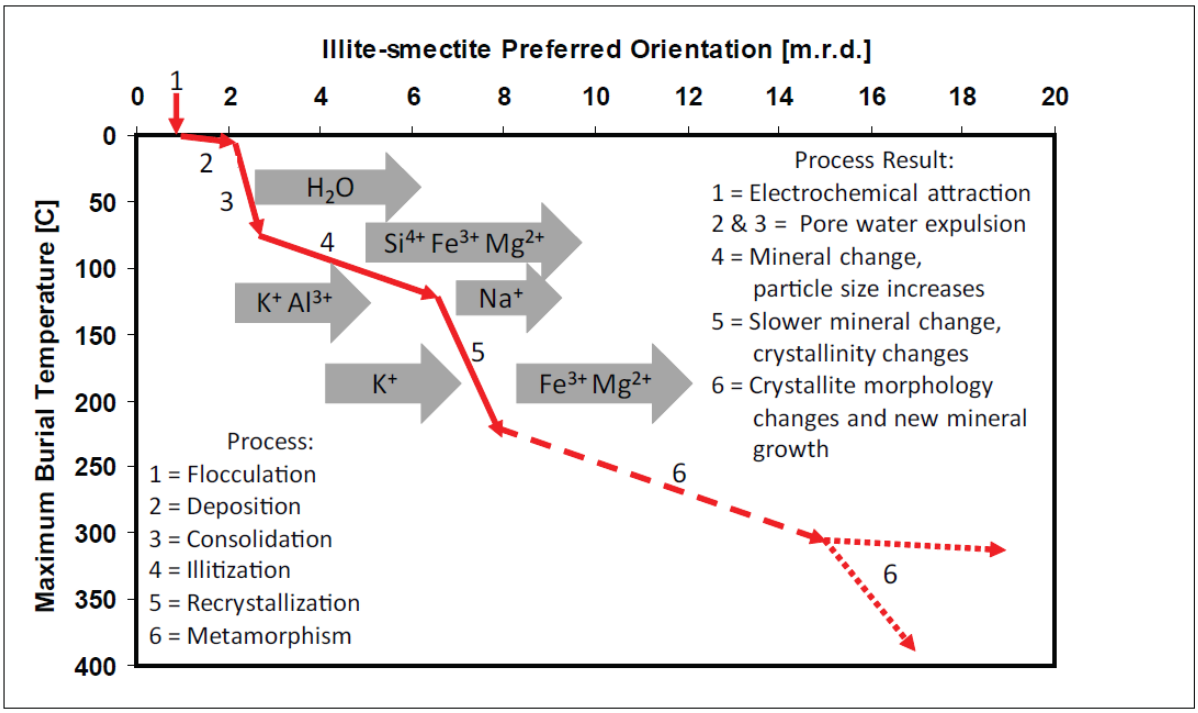

Figure 9. The development of illite-smectite preferred orientation is a stepwise process (Modified from Haines et al. 2009). Mechanical processes give way to chemical processes that see initial significant changes in mineralogy and associated preferred orientation. As reaction products are consumed diagenesis slows but potassium is still taken up by clay minerals that concomitantly release iron and aluminum (mica formation). A second significant stage of preferred orientation development occurs into metamorphism but is not well defined.

8. References

Ahn, J.H. and Peacor, D.R., 1986. Transmission and analytical electron microscopy of the smectite to illite transition. Clays and Clay Minerals, 34: 165-179.

Anczkiewicz, A., 2006. Verification by AFT technique of the maxium palaeotemperatures evaluted from illite-smectite for the Tatra Mts., the Podhale Basin and the neighbouring area of the Outer Carpathians. PhD thesis, Institute of Geological Sciences PAN, Krakow (in Polish).

Aplin, A.C., Matenaar, I.F., McCarty, D.K. and van der Pluijm, B.A., 2006. Influence of mechanical compaction and clay mineral diagenesis on the microfabric and pore-scale properties of deep-water Gulf of Mexico mudstones. Clays and Clay Minerals, 54(4): 500-514.

Bell, T.E., 1986. Microstructure in mixed-layer illite/smectite and its relationship to the reaction of smectite and illite. Clays and Clay Minerals, 34(2): 146-154.

Bjørlykke, K. and Høeg, K., 1997. Effects of burial diagenesis on stresses, compaction and fluid flow in sedimentary basins. Marine and Petroleum Geology, 14(3): 267-276.

Boles, J.R. and Franks, S.G., 1979. Clay diagenesis in Wilcox Sandstones of southwest Texas. Journal of Sedimentary Petrology, 49: 55-70.

Bowers, G.L., 1995. Pore Pressure Estimation From Velocity Data: Accounting for Overpressure Mechanisms Besides Undercompaction. Society of Petroleum Engineers (SPE 27488), 10(2): 89-95.

Brusewitz, A.M., 1986. Chemical and Physical-Properties of Paleozoic Potassium Bentonites from Kinnekulle, Sweden. Clays and Clay Minerals, 34(4): 442-454.

Cliff, G. and Lorimer, G.W., 1975. Quantitative-Analysis of Thin Specimens. Journal of Microscopy-Oxford, 103(MAR): 203-207.

Curtis, C.D., Lipshie, S.R., Oertel, G. and Pearson, M.J., 1980. Clay Orientation in Some Upper Carboniferous Mudrocks, Its Relationship to Quartz Content and Some Inferences About Fissility, Porosity and Compactional History. Sedimentology, 27(3): 333-339.

Day-Stirrat, R.J., Aplin, A.C., Środoń, J. and van der Pluijm, B.A., 2008a. Diagenetic reorientation of phyllosilicate minerals in Paleogene mudstones of the Podhale Basin, southern Poland. Clays and Clay Minerals, 56(1): 100-111.

Day-Stirrat, R.J., Loucks, R.G., Milliken, K.L., Hillier, S. and van der Pluijm, B.A., 2008b. Phyllosilicate orientation demonstrates early timing of compactional stabilization in calcite-cemented concretions in the Barnett Shale (Late Mississippian), Fort Worth Basin, Texas (U.S.A). Sedimentary Geology, 208(1-2): 27-35.

Day-Stirrat, R.J. et al., 2011. Preferred orientation of phyllosilicates: Effects of composition and stress on resedimented mudstone microfabrics. Journal of Structural Geology, 33: 1347-1358.

Djéran-Maigre, I., Tessier, D., Grunberger, D., Velde, B. and Vasseur, G., 1998. Evolution of microstructures and of macroscopic properties of some clays during experimental compaction. Marine and Petroleum Geology, 15(2): 109-128.

Goulty, N.R. and Sargent, C., 2016. Compaction of diagenetically altered mudstones – Part 2: Implications for pore pressure estimation. Marine and Petroleum Geology, 77: 806-818.

Goulty, N.R., Sargent, C., Andras, P. and Aplin, A.C., 2016. Compaction of diagenetically altered mudstones – Part 1: Mechanical and chemical contributions. Marine and Petroleum Geology, 77: 703-713.

Haines, S.H., van der Pluijm, B.A., Ikari, M.J., Saffer, D.M. and Marone, C., 2009. Clay fabric intensity in natural and artificial fault gouges: Implications for brittle fault zone processes

635 and sedimentary basin clay fabric evolution. Journal of Geophysical Research-Solid
636 Earth, 114.
637 Ho, N.C., Peacor, D.R. and van der Pluijm, B.A., 1995. Reorientation Mechanisms of
638 Phyllosilicates in the Mudstone-to-Slate Transition at Lehigh Gap, Pennsylvania. Journal
639 of Structural Geology, 17(3): 345-356.
640 Ho, N.C., Peacor, D.R. and van der Pluijm, B.A., 1999. Preferred Orientation of Phyllosilicates
641 in Gulf Coast Mudstones and Relation to the Smectite-Illite Transition. Clays and Clay
642 Minerals, 47(4): 495-504.
643 Hover, V.C., Walter, L.M., Peacor, D.R. and Martini, A.M., 1999. Mg-Smectite Authigenesis in
644 a Marine Evaporite Environment, Salina Ometepec, Baja California. Clays and Clay
645 Minerals, 47(3): 252-268.
646 Hower, J., Eslinger, E.V., Hower, M.E. and Perry, E.A., 1976. Mechanism of Burial
647 Metamorphism of Argillaceous Sediment 1. Mineralogical and Chemical Evidence.
648 Geological Society of America Bulletin, 87(5): 725-737.
649 Inoue, A., Kohyama, N., Kitagawa, R. and Watanabe, T., 1987a. Chemical and morphological
650 evidence for the conversion of smectite to illite. Clays and Clay Minerals, 42: 276-287.
651 Inoue, A., Velde, B., Meunier, A. and Touchard, G., 1987b. Mechanism of illite formation
652 during smectite-to-illite conversion in a hydrothermal system. American Mineralogist,
653 73: 1325-34.
654 Jacob, G., Kisch, H.J. and van der Pluijm, B.A., 2000. The relationship of phyllosilicate
655 orientation, X-ray diffraction intensity ratios, and c/b fissility ratios in metasedimentary
656 rocks of the Helvetic zone of the Swiss Alps and the Caledonides of Jamtland, central
657 western Sweden. Journal of Structural Geology, 22(2): 245-258.
658 Jiang, W.T., Peacor, D.R., Merriman, R.J. and Roberts, B., 1990. Transmission and Analytical
659 Electron-Microscopic Study of Mixed-Layer Illite Smectite Formed as an Apparent
660 Replacement Product of Diagenetic Illite. Clays and Clay Minerals, 38(5): 449-468.
661 Jiang, W.T., Peacor, D.R. and Buseck, P.R., 1994. Chlorite geothermometry?-contamination and
662 apparent octahedral vacancies. Clays and Clay Minerals, 42(5): 593-605.
663 Kim, J., Dong, H.L., Seabaugh, J., Newell, S.W. and Eberl, D.D., 2004. Role of microbes in the
664 smectite-to-illite reaction. Science, 303(5659): 830-832.
665 Kim, J.W., Peacor, D.R., Tessier, D. and Elsass, F., 1995. A Technique for Maintaining Texture
666 and Permanent Expansion of Smectite Interlayers for Tem Observations. Clays and Clay
667 Minerals, 43(1): 51-57.
668 Klimentidis, R.E. and Mackinnon, I.D.R., 1986. High-Resolution Imaging of Ordered Mixed-
669 Layer Clays. Clays and Clay Minerals, 34(2): 155-164.
670 Lahann, R., 2002. Impact of smectite diagenesis on compaction modeling and compaction
671 equilibrium. In: A.R. Huffman and G.L. Bowers (Editors), American Association of
672 Petroleum Geologists Memoir 76: Pressure regimes in sedimentary basins and their
673 prediction. American Association of Petroleum Geologists, Tulsa, Oklahoma, pp. 61-72.
674 Lahann, R.W. and Swarbrick, R.E., 2011. Overpressure generation by load transfer following
675 shale framework weakening due to smectite diagenesis. Geofluids, 11(4): 362-375.
676 Land, L.S., Mack, L.E., Milliken, K.L. and Lynch, F.L., 1997. Burial diagenesis of argillaceous
677 sediment, south Texas Gulf of Mexico sedimentary basin: A reexamination. Geological
678 Society of America Bulletin, 109(1): 2-15.
679 Land, L.S. and Milliken, K.L., 2000. Regional loss of SiO2, and gain of K2O during burial
680 diagenesis of Gulf Coast mudrocks, USA. In: R.H. Worden and S. Morad (Editors),

681 Quartz Cementation in Sandstones. International Association of Sedimentologists, pp.
682 183-197.
683 Li, G.J., Peacor, D.R. and Coombs, D.S., 1997. Transformation of smectite to illite in bentonite
684 and associated sediments from Kaka Point, New Zealand: Contrast in rate and
685 mechanism. Clays and Clay Minerals, 45(1): 54-67.
686 Marynowski, L. et al., 2006. Origin of organic matter from tectonic zones in the Western Tatra
687 Mountains Crystalline Basement, Poland: An example of bitumen - source rock
688 correlation. Marine and Petroleum Geology, 23(2): 261-279.
689 Masuda, H., Peacor, D.R. and Dong, H., 2001. Transmission electron microscopy study of
690 conversion of smectite to illite in mudstones of Nankai Trough: contrast with coeval
691 bentonites. Clays and Clay Minerals, 49(2): 109-118.
692 Merriman, R.J., Roberts, B., Peacor, D.R. and Hirons, S.R., 1995. Strain-Related Differences in
693 the Crystal-Growth of White Mica and Chlorite - a Tem and Xrd Study of the
694 Development of Metapelitic Microfabrics in the Southern Uplands Thrust Terrane,
695 Scotland. Journal of Metamorphic Geology, 13(5): 559-576.
696 Merriman, R.J. and Peacor, D.R., 1998. Very low-grade metapelites: mineralogy, microfabrics
697 and measuring reaction progress. In: M. Frey and D. Robinson (Editors), Low-Grade
698 Metamorphism. Blackwell Science.
699 Merriman, R.J., 2002. Contrasting clay mineral assemblages in British Lower Palaeozoic slate
700 belts: the influence of geotectonic setting. Clay Minerals, 37(2): 207-219.
701 Moore, D.M. and Reynolds, R.C.J., 1997. X-ray diffraction and the identification and analysis of
702 clay minerals. Oxford University Press, Oxford, New York.
703 Nadeau, P.H., Peacor, D.R., Yan, J. and Hillier, S., 2002. I-S precipitation in pore space as the
704 cause of geopressuring in Mesozoic mudstones, Egersund Basin, Norwegian Continental
705 Shelf. American Mineralogist, 87(11-12): 1580-1589.
706 Oertel, G. and Curtis, C.D., 1972. Clay-Ironstone Concretion Preserving Fabrics Due to
707 Progressive Compaction. Geological Society of America Bulletin, 83(9): 2597-2605.
708 Olszewska, B.W. and Wieczorek, J., 1998. The Palaeogene of the Podhale Basin (Polish Inner
709 Carpathians)-micropaleontological perspectives. Przeglad Geologiczny, 46(8/2): 721-
710 728.
711 Peacor, D.R., 1992. Analytical Electron-Microscopy - X-Ray-Analysis. Reviews in Mineralogy,
712 27: 113-140.
713 Perry, E. and Hower, J., 1970. Burial diagenesis in Gulf Coast pelitic sediments. Clays and Clay
714 Minerals, 18: 165-177.
715 Poprawa, P. and Marynowski, L., 2005. Thermal history of the Podhale Trough (northern part of
716 the Central Carpathian Paleogene Basin) - preliminary results from 1-D maturity
717 modeling. Mineralogical Society of Poland - Special Papers, 25: 352-355.
718 Ramseyer, K. and Boles, J.R., 1986. Mixed-Layer Illite Smectite Minerals in Tertiary Sandstones
719 and Shales, San-Joaquin Basin, California. Clays and Clay Minerals, 34(2): 115-124.
720 Rieke, H.H. and Chilingarian, G.V., 1974. Compaction of argillaceous sediments. Compaction of
721 argillaceous sediments. Developments in Sedimentology 16. Elsevier.
722 Sorby, H.C., 1853. On the origin of slaty cleavage. Edinburgh New Philosophical Journal, 10:
723 136.
724 Środoń, J., Morgan, D.J., Eslinger, E.V., Eberl, D.D. and Karlinger, M.R., 1986. Chemistry of
725 Illite Smectite and End-Member Illite. Clays and Clay Minerals, 34(4): 368-378.

Środoń, J., Clauer, N., Banas, M. and Wojtowicz, A., 2006a. K-Ar evidence for a Mesozoic thermal event superimposed on burial diagenesis of the Upper Silesia Coal Basin. Clay Minerals, 41(2): 669-690.
Środoń, J. et al., 2006b. Diagenetic history of the Podhale-Orava Basin and the underlying Tatra sedimentary structural units (Western Carpathians): evidence from XRD and K-Ar of illite-smectite. Clay Minerals, 41: 751-774.
Środoń, J., 2009. Quantification of illite and smectite and their layer charges in sandstones and shales from shallow burial depth. Clay Minerals, 44: 421-434.
Stuart, A., Ord, J.K. and Arnold , S., 1999. Kendall's Advanced Theory of Statistics, Volume 2A, London : Arnold ; New York : Oxford University Press.
Tari, G., Baldi, T. and Baldibeke, M., 1993. Paleogene Retroarc Flexural Basin beneath the Neogene Pannonian Basin - a Geodynamic Model. Tectonophysics, 226(1-4): 433-455.
Taylor, T.R. et al., 2010. Sandstone diagenesis and reservoir quality prediction: Models, myths, and reality. AAPG Bulletin, 94(8): 1093-1132.
van de Kamp, P.C., 2008. Smectite-Illite-Muscovite transformation, Quartz Dissolution, and Silica Release in Shales. Clays and Clay Minerals, 56(1): 66-81.
van der Pluijm, B.A., Lee, J.H. and Peacor, D.R., 1988. Analytical Electron-Microscopy and the Problem of Potassium Diffusion. Clays and Clay Minerals, 36(6): 498-504.
Voltolini, M., Wenk, H.R., Mondol, N.H., Bjorlykke, K. and Jahren, J., 2009. Anisotropy of experimentally compressed kaolinite-illite-quartz mixtures. Geophysics, 74(1): D13-D23.
Warren, E.A. and Ransom, B., 1992. The Influence of Analytical Error Upon the Interpretation of Chemical Variations in Clay-Minerals. Clay Minerals, 27(2): 193-209.
Weaver, C.E., 1989. Clays, muds, and shales. Developments in Sedimentology 44. Elsevier, Amsterdam, New York.
Westwalewicz-Magilska, E., 1986. Nowe spojrzenie na geneze osadów fliszu podhalanskiego. Przeglad Geologiczny, 12: 690-698 (in Polish).
Yang, Y. and Aplin, A.C., 2004. Definition and practical application of mudstone porosity–effective stress relationships. Petroleum Geoscience, 10(2): 153-162.
Yang, Y.L. and Aplin, A.C., 1997. A method for the disaggregation of mudstones. Sedimentology, 44(3): 559-562.